

Effect of Metallic Li on the Corrosion Behavior of Inconel 625 in Molten LiCl-Li₂O-Li

William Phillips,^{1,*} Zachary Karmiol,^{1,2,*} and Dev Chidambaram ^{6,3,**,z}

¹Materials Science and Engineering, University of Nevada, Reno, Nevada 89557-0388, USA

The corrosion behavior of Inconel 625 in molten LiCl solutions maintained at 650° C and containing various quantities of Li₂O and metallic Li was studied for possible application in the electroreduction of used oxide-based nuclear fuel. This study focusses on the morphological and elemental changes on the surface of the samples with an emphasis on cross-sectional analyses conducted using focused ion beam microscopy. In the absence of metallic Li, a stable oxide film is formed that limits the corrosion of the base material to 0.07mm/year. However, in the presence of metallic Li, the formation of this film is impeded, resulting in dealloying of the base material and the formation of a highly porous microstructure composed primarily of Ni.

© The Author(s) 2019. Published by ECS. This is an open access article distributed under the terms of the Creative Commons Attribution Non-Commercial No Derivatives 4.0 License (CC BY-NC-ND, http://creativecommons.org/licenses/by-nc-nd/4.0/), which permits non-commercial reuse, distribution, and reproduction in any medium, provided the original work is not changed in any way and is properly cited. For permission for commercial reuse, please email: oa@electrochem.org. [DOI: 10.1149/2.0201906jes]



Manuscript submitted January 31, 2019; revised manuscript received March 7, 2019. Published April 3, 2019.

In order to reprocess used nuclear fuel (UNF) from light water reactors using pyrometallurgical techniques, a reduction operation is necessary to convert UO₂-based UNF into a metallic product that can then be processed in subsequent unit operations. 1-5 The prototypical process by which the reduction of UO₂ is conducted is via the electrolytic reduction operation developed at Argonne National Laboratory (ANL).^{2,6} In this process, LiCl containing 1 to 2wt% Li₂O and maintained at 650°C serves as the electrolyte. 7,8 The reduction is performed with UNF loaded in a stainless steel cathode basket which is polarized vs. a suitable anode, typically made of Pt, either galvanostatically or potentiostatically.^{3,9} To achieve high reduction yields, it has been shown by a number of researchers that it is necessary to polarize UO₂ at potentials beyond the electrochemical window of Li₂O, which results in the formation of metallic Li at the cathode. 3,9,10 Some of the metallic Li thus generated then metalothermically reduces the UNF in the cathode; however, LiCl is capable of solvating Li to a limited degree, which leads to the formation of a tertiary LiCl-Li₂O-Li electrolyte. ^{3,9,10} As the process goes to completion, the electrolyte eventually reaches Li saturated conditions, and may even form and be present as clusters.11

The dissolution of alkali metals in their respective alkali halides has been well studied over the last century, notably by M.A. Bredig at Oak Ridge National Laboratory, among others. 12-14 The two primary models of alkali metal - alkali halide systems are the f- center model and the sub-halide model. 13 In the f- center model typical for alkali metal - alkali halide systems, the excess electron is delocalized from any particular cation core, leaving a free electron that imparts a metallic character to the molten solution. 13 This leads to several orders of magnitude increase in electrical conductivity of solution as the concentration of the alkali metal increases toward saturation, as well as causing a number of other changes in physical and chemical properties. The sub-halide model is typically representative of transition metals and post-transition metals in their respective halides and gives rise to the formation of abnormally reduced species due to the formation of complex molecules that keep electrons localized to the molecular scale, as is typical for the Bi-BiCl₃ system. ¹³ Sub-halide forming systems are not associated with an increase in electrical conductivity in the same manner as the f- center model predicts. Other dissolution mechanisms have also been reported, such as the formation of colloidal suspensions of nanoclusters of Na2 or Li8 in the Na-NaCl and Li-LiCl systems, respectively. 11,13 It is important to note that none of these effects are mutually exclusive, and it is possible that the

simultaneous action of multiple dissolution mechanisms may occur simultaneously in the same system. Of the alkali metal – alkali halide systems, the Li-LiCl system has proven to be particularly challenging in the determination of the solubility limit of the metal in the metal salt, with the apparent solubility limit seeming to vary depending on the experimental methods; however, approximately 0.3wt% has been shown to be a useful estimate at the temperatures of the electrolytic reduction operation. ^{12,13,15–19} Importantly, the concentration of Li₂O has been shown to have minimal effect on the measured solubility limit of Li in LiCl-Li₂O. ¹⁹ The discrepancy between the various reported values of the solubility limit of Li in LiCl may be due to the simultaneous action of the various dissolution mechanisms theorized for this system. ¹¹

For the electrolytic reduction of UNF to be implemented on a large scale, knowledge of the degradation of materials in contact with the electrolyte is necessary, particularly for the container material. Corrosion in molten LiCl-Li₂O under inert or oxidizing atmospheres has been fairly well studied, and the corrosion of various materials has been found to follow similar mechanisms to those observed in other molten salt systems.^{20–26} Primarily, the dissolution of alloying elements, and consequently the corrosion rate, is governed primarily by the activity of the O²⁻ ion in the solution according to the Lux-Flood model of salt basicity, as well as by the presence of impurities such as moisture or transition metal halides. 20,27,28 For the electroreduction process, such models are insufficient to completely describe corrosion due to the presence of dissolved Li. To date, very few investigations into the effects of Li on the corrosion of materials exposed to this system have been performed.^{29–34} The initial studies conducted by Indocochea, et al. conflicted with studies conducted by Mishra and Olson due to widely varying experimental parameters, leading to confusion about the effect Li had on the degradation observed. ^{29,30} Recent studies have been performed to address these issues, but were of short term in nature and did not investigate the degradation of the materials studied in cross section. 31-33 These studies showed that a transition from molten salt based corrosion to a liquid metal attack induced degradation occurred at approximately 0.6wt%Li, and that the concentration of both Li and Li₂O affected the corrosion processes that were observed. Recent work by researchers at the Korean Atomic Energy Research Institute showed that Ni displayed minimal corrosion in the absence of Li, but underwent significant degradation in the presence of metallic Li. 34 In this light, the current study investigates the corrosion behavior of Inconel 625 (I625) in the LiCl-Li₂O-Li system at 650°C. To understand the effect of oxide concentration, metal concentration and the period of exposure, the solution chemistries studied consisted of LiCl containing 1 or 2wt% Li₂O and 0, 0.3, 0.6, or 1wt% Li, with samples exposure periods of 500 and 1000hr. This study focusses on the

²University of Nevada, Reno Electron Microscopy and Microanalysis Facility, Reno, Nevada, USA

³Nevada Institute For Sustainability, Reno, Nevada 89557-0388, USA

^{*}Electrochemical Society Student Member.

^{**}Electrochemical Society Member.

^zE-mail: dcc@unr.edu

observed degradation of I625 under these conditions by determining the changes to the microstructure and elemental composition using scanning electron microscopy (SEM) coupled with energy dispersive X-ray spectroscopy (EDS) of the sample surfaces as well as their cross sections.

Experimental

Experiments were conducted in a Vacuum Atmospheres OMNI-LAB glove box under Ar containing less than 2ppm O_2 and less than 1ppm H_2O . Anhydrous LiCl, Li₂O, and Ni crucibles were obtained from Alfa-Aesar and were of 99%, 99.5%, and 99% purity, respectively. Li metal of 99% purity was purchased from Strem Chemicals. I625 coupons were cut from a 3.175mm thick plate obtained from High Performance Alloys. The composition of this alloy as measured via the EDS used for cross sectional investigation was 62.3wt% Ni 23.5wt% Cr, 6.5wt% Mo, 5.1% Fe, and 2.6wt% Nb.

Studies were conducted using duplicate samples, and 500 hour and 1000 hour exposures were conducted in parallel, with the 500 hour samples removed from the experiment upon completion of the allotted exposure period. A 6.5 inch inner diameter, 6 inch tall cylindrical heater from Watlow (1500 watts) was used to maintain a temperature of $650 \pm 5^{\circ}\mathrm{C}$ for the duration of the exposure period. A 6 inch diameter graphite block was machined to accommodate 5 Ni crucibles, with slots machined to accommodate the sample hanging rods. This configuration allowed for repeatable placement of the samples within the melt during the salt replacement procedure outlined below. Two identical furnaces were constructed to maximize the number of experiments that could be ran in parallel. In operation, four experiments were ran simultaneously in each furnace, which allowed for the extra 5^{th} crucible location to be used for salt replacement purposes.

Prior to exposure, the metal samples were cut into 1.27cm by 1.27cm squares using a CO_2 laser. The samples were then polished to a 1 μ m surface finish on both sides using a diamond abrasive and spot welded to loops of SS316L wire for suspension from the sample hanging rods, as was performed in our previous studies. 31–33 Sample hanging rods were made of like material to the samples, as alumina rods proved to be incapable of withstanding the highly reducing atmosphere directly over the molten solutions containing metallic Li for the duration of these experiments. The mass of each sample was recorded immediately prior to exposure.

Considering the evaporation of Li and Li₂O over time that was observed in other short-term studies and the extended exposure periods of this study, the salt charge for each test was replaced at a period of once every 96 hours to maintain the solution chemistry. 31–33,35,36 To minimize the effects of impurity H₂O, LiCl was dried in a vacuum oven in air at 200°C for 24 hours before being transferred into the glove box for storage.^{31,37} Immediately prior to insertion in the primary furnace, a cleaned Ni crucible containing the weighed amount of LiCl was dried under Ar for 2hr in a dedicated furnace maintained at 550°C. After insertion into the primary furnace, the LiCl was allowed 1 hour to reach thermal equilibrium, after which time the required mass of Li₂O and Li were added to the molten salt by placing the Li₂O powder and Li pellets on top of the solution. Total salt mass contained in each crucible was 50g. The melt was allowed to equilibrate for another hour prior to the transfer of the corrosion specimens from the old salt charge to the new salt charge. As the concentration of Li was above the solubility limit for the 0.6 and 1wt% tests, a significant fraction was likely present as a colloidal suspension. Sample transfer was accomplished via specially fabricated tongs, which allowed for the transfer time to be less than 5 seconds on average. Following transfer of the samples to the new salt charge, the old salt charge was removed from the furnace and allowed to cool to room temperature. The cooled salt ingot was then dissolved in deionized (DI) water. The Ni crucible was then sanded with 600 grit SiC paper, rinsed with DI water, cleaned with isopropyl alcohol, and dried under vacuum prior to re-use for the next salt charge for the same solution chemistry conditions. Two Ni crucibles were alternated between for each solution chemistry.

Following completion of the exposure period, the samples were removed from the furnace and allowed to cool to room temperature in the glove box atmosphere. All samples were stored in the Ar glove box between analytical procedures. As it was unknown if the surface films formed on the corrosion specimens would be stable in atmosphere, surface analysis was performed both prior to and following removal of the residual salt layer. Following the initial surface analytical procedures, residual LiCl was removed by placing each sample in 25ml of HPLC grade methanol for 15 minutes with constant agitation. Prior to the methanol rinsing procedure, all surface analysis was performed under inert atmosphere or vacuum conditions, depending on technique. The data presented here were collected following the methanol rinsing procedure, as the residual salt layer significantly interfered with surface analysis as has been described earlier.³¹ No chemical or morphological changes were observed as a result of the methanol rinsing procedure. Gravimetric weight change measurements were performed following the methanol rinsing procedure.

All samples exposed to Li containing melts were cross sectioned using a Buehler cubic-BN wafering blade on a slow speed saw and polished according to Buehler's recommended polishing techniques to a $0.05\mu m$ surface finish prior to analysis. Samples exposed to LiCl-Li₂O in the absence of Li were investigated using only FIB milling for cross sectional analysis due to the relatively shallow depth of attack.

SEM of the sample surfaces was performed using a Hitachi S-4700 and EDS data was collected via the attached Oxford Instruments energy dispersive X-ray spectrometer. The electron beam was operated at an accelerating voltage of 5kV for surface morphology images, while 20kV was used for collection of EDS spectra. Emission current was maintained at 10mA. FIB milling and subsequent SEM-EDS analysis for cross sectional images was performed using a FEI Scios dual-beam FIB/SEM equipped with a TEAM Pegasus Integrated EDS-EBSD. The same dual-beam FIB/SEM was used to perform the SEM-EDS analysis of all of the cross sectioned samples, including those mechanically cross sectioned and polished. The electron beam was operated at 20kV for both imaging and EDS analysis.

The exposed surface area was calculated based on the measured submersion depth of each sample. The average corrosion rate in mm/year and the mass loss rate in mg cm⁻² hr⁻¹ was then calculated based on the mass change, density of the alloy, exposed surface area, and length of exposure.

Results

The surface of I625 samples exposed to LiCl-Li₂O solutions in the absence of Li displayed a high degree of crystallinity indicative of a well-formed oxide layer, while the surfaces of samples exposed to LiCl-Li₂O in the presence of metallic Li showed a very porous, almost sponge-like microstructure. To illustrate these points, the SEM micrographs taken of the I625 samples exposed to LiCl-1wt%Li₂O containing 0, 0.3, 0.6, or 1wt%Li for 500hr are shown in Figure 1.

In the absence of Li, the oxide layer is well formed and shows evidence of a multi layered structure that is discussed in greater detail below. EDS analysis of the area shown in Figure 1a showed that the surface was composed of 22at% Cr, 66at%O, and 13at%Ni, with minor quantities of other elements, indicating a primarily Cr based oxide layer. Li is not detectable via EDS, however, spectroscopic analysis has definitively shown this compound to be LiCrO₂.³⁸ The presence of Li in the molten LiCl-Li₂O solution destabilizes the oxide layer and forms a very porous microstructure that is similar in appearance to a Ni foam. EDS analysis of these areas consistently showed greater than 80at%Ni, with high depletion of Cr, Mo, and Nb, although the Ni:Fe ratio remained close to that of the base material. There was little difference between the microstructures observed at low and high Li concentrations, with the microstructure of the I625 samples exposed to melts containing 0.3wt%Li displaying microstructures nearly identical to samples exposed to melts containing 1wt%Li. Exposure periods of 500hr and 1000hr both yielded nearly indistinguishable microstructures, as can be observed by comparing the micrographs of I625 samples exposed to LiCl-1wt%Li2O containing 0, 0.3, 0.6, and

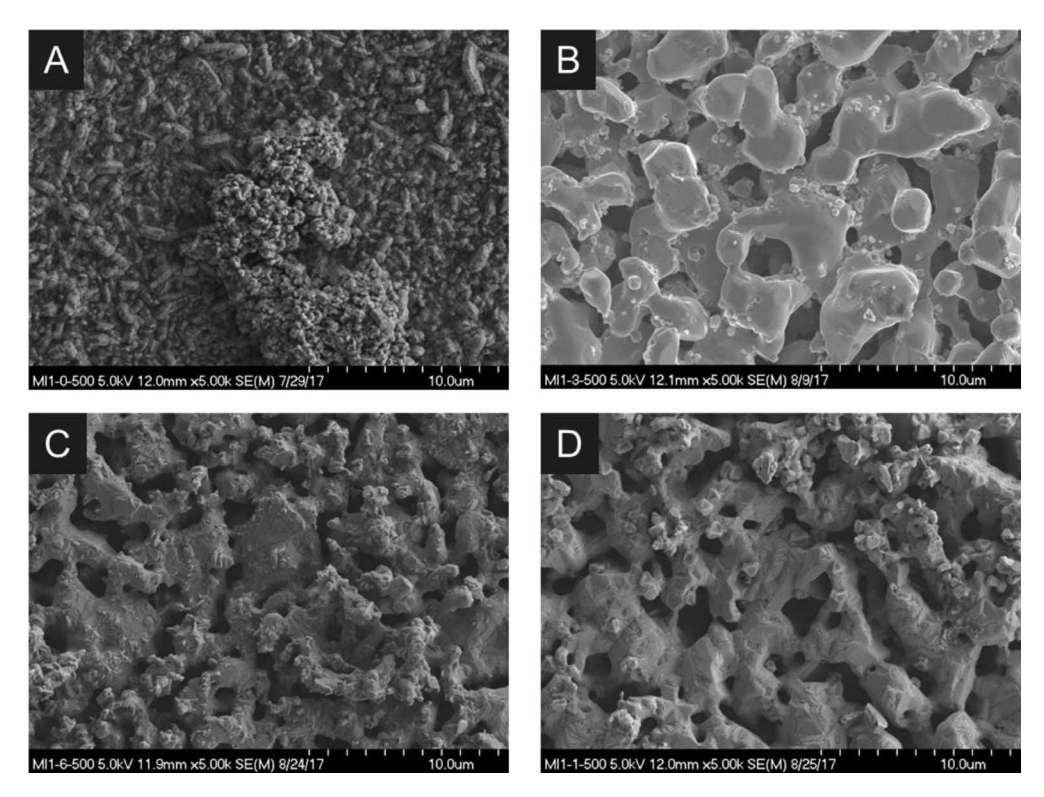
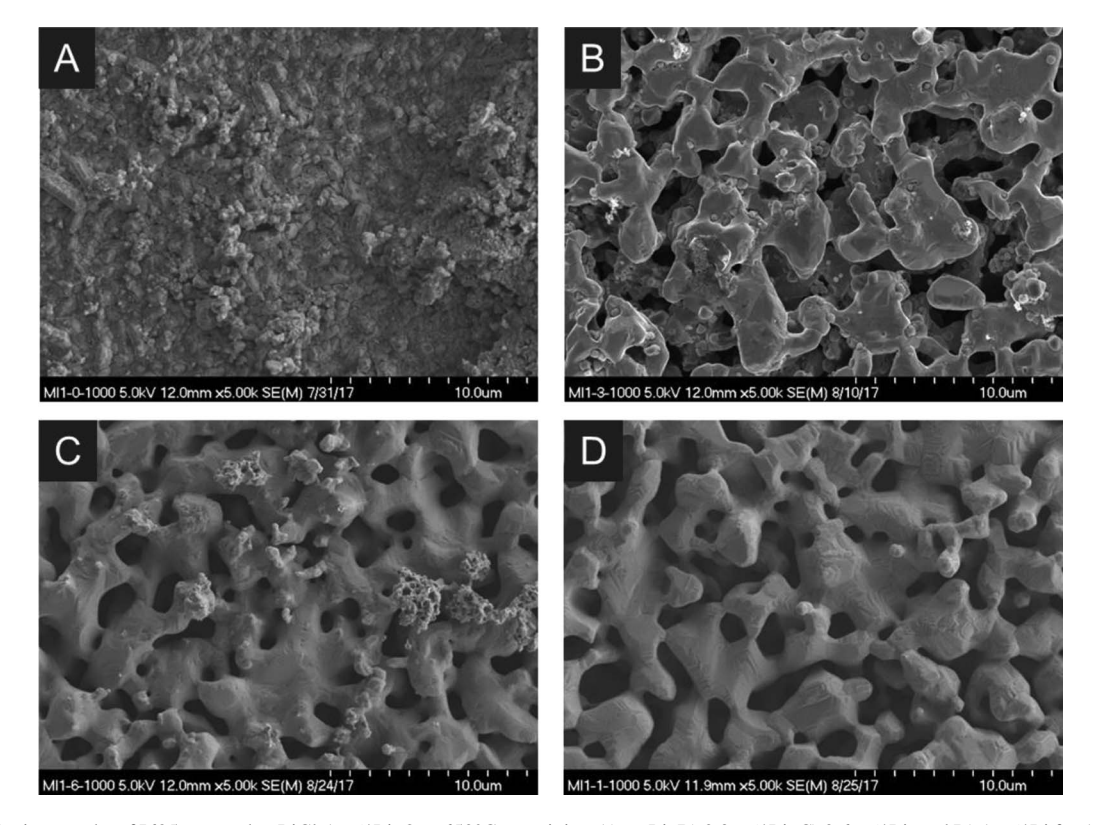


Figure 1. SEM micrographs of I625 exposed to LiCl-1wt%Li₂O at 650°C containing A) no Li, B) 0.3wt%Li, C) 0.6wt%Li, and D) 1wt%Li for 500hr and rinsed with methanol.



 $\textbf{Figure 2.} \hspace{0.2cm} \textbf{SEM} \hspace{0.2cm} \textbf{micrographs} \hspace{0.2cm} \textbf{of} \hspace{0.2cm} \textbf{I625} \hspace{0.2cm} \textbf{exposed} \hspace{0.2cm} \textbf{to} \hspace{0.2cm} \textbf{LiCl-1wt\%Li}_2 O \hspace{0.2cm} \textbf{at} \hspace{0.2cm} \textbf{650}^{\circ} \textbf{C} \hspace{0.2cm} \textbf{containing} \hspace{0.2cm} \textbf{A)} \hspace{0.2cm} \textbf{no} \hspace{0.2cm} \textbf{Li,} \hspace{0.2cm} \textbf{B)} \hspace{0.2cm} \textbf{0.3wt\%Li,} \hspace{0.2cm} \textbf{C)} \hspace{0.2cm} \textbf{0.6wt\%Li,} \hspace{0.2cm} \textbf{and} \hspace{0.2cm} \textbf{D)} \hspace{0.2cm} \textbf{1wt\%Li} \hspace{0.2cm} \textbf{for} \hspace{0.2cm} \textbf{1000hr} \hspace{0.2cm} \textbf{and} \hspace{0.2cm} \textbf{rinsed} \hspace{0.2cm} \textbf{with} \hspace{0.2cm} \textbf{methanol.} \\ \textbf{1000hr} \hspace{0.2cm} \textbf{1000hr} \hspace{0$



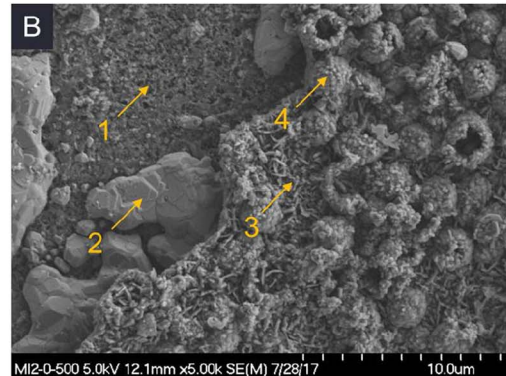


Figure 3. SEM micrographs taken at (A) low magnification and (B) high magnification of the highlighted area on the I625 sample exposed to LiCl-2wt%Li₂O-0wt%Li at 650°C for 500hr after methanol rinsing. The delamination of the outer surface layer on this sample provided a unique opportunity to examine the layered structure of the oxide films that form on I625 upon exposure to molten LiCl-Li₂O in the absence of Li. The compositions of Layers 1 through 4 in image B were obtained via EDS analysis and are given in Table II, below.

1wt%Li for 1000hr shown in Figure 2 to the micrographs presented in Figure 1.

Variations in Li_2O concentration and exposure length did not dramatically alter the morphology observed on I625 samples exposed to LiCl-Li $_2\text{O}$ -Li compared to those shown in Figures 1 and 2. Consistent morphology was observed in the presence of Li, with all samples displaying similar structures. Likewise, in the absence of Li, a well-developed, highly crystalline oxide layer was consistently observed. Additionally, the surface of the I625 sample exposed to LiCl-2wt%Li $_2\text{O}$ -0wt%Li for 500hr had a small number of locations where the oxide layer had partially delaminated, which allowed for direct observation of the layered structure of the oxide films formed on I625 during exposure to LiCl-Li $_2\text{O}$ in the absence of Li. SEM micrographs of one of these locations are shown in Figure 3, and the compositions of locations 1 through 4 detected via EDS are given in Table I.

The presence of a multilayered oxide structure is easily discernable in this image. Each layer was analyzed using EDS at the spots marked by the arrows. The layers were numbered 1 through 4 starting with the innermost and proceeding outward. Due to the composition of Layer 2 and the lack of Ti in both Layers 1 and 2, which is present as an impurity in the Li₂O used in this study, it is thought that Layer 1 is the result of the inward diffusion of O into the base material. The O concentration of Layer 2 is much lower than in any of the other layers observed here, and its composition is the most similar to the base alloy, although all areas analyzed were notably depleted in Mo and Nb. The size of the grains in Layer 2 and their relative orientations are also similar to the morphology of the I625 samples exposed to LiCl-Li₂O in the presence of Li, as can be observed by comparison with Figures 1 and 2, indicating that this is likely the base material

Table I. EDS compositional analysis obtained for locations 1 through 4 marked in Figure 3B for the I625 sample exposed to LiCl-2wt%Li₂O-0wt%Li at 650° C for 500hr.

Element	Layer 1 Atomic%	Layer 2 Atomic%	Layer 3 Atomic%	Layer 4 Atomic%
C				5.07
O	62.43	11.22	61.07	65.48
Mg	1.35		2.56	3.14
Cl	0.41		0.27	0.47
Cr	18.34	3.33	12.99	20.07
Fe	0.61	3.74	1.21	0.32
Ni	15.23	80.97	21.44	5.13
Nb	0.9			
Mo	0.73	0.74		
Ti			0.46	0.32

which has been depleted in Cr to facilitate the outward growth of Layers 3 and 4. These outermost layers differ in both morphology and composition, suggesting a difference in the compounds that compose them. Layer 3 is the layer closest to the base material, and has a plate-like morphology. The high Ni content of Layer 3 compared to Layer 4 implies that Layer 3 is composed of primarily NiFe_xCr_{2-x}O₄ with a relatively low value of x, while Layer 4 is primarily LiCrO₂ based. Both Layer 3 and Layer 4 have incorporated Ti from the impurities present in the Li₂O used in this study. The spheroidal morphology of Layer 4 suggests that its growth begins at specific nucleation sites. Some of these spheroids from Layer 4 appear to be broken or incompletely formed, showing that they are hollow. Figure 4 shows the results of EDS mapping of Ni, Fe, Cr, and O for the same location shown in Figure 3 which further highlights the differences between the layers observed on this sample.

Cross section SEM-EDS.—The cross sections of the samples were investigated to determine the depth to which the degradation of the surface penetrated into the bulk of the sample. In the absence of Li, the penetration into the bulk of the sample was minimal, as evidenced by Figures 5 and 6, which show the FIB milled cross section of the I625 samples exposed to LiCl-1wt%Li₂O-0wt%Li at 650°C for 500hr and 1000hr, respectively. Small pores of less than 2µm in diameter were observed immediately below the outer oxide layer for the 500hr sample, corresponding to a layer of Mo enrichment as evidenced in Figure 5d. As shown in the EDS analysis of this sample previously, the oxide layer does not incorporate a significant amount of Mo, indicating that the surface enrichment of Mo is deleterious to the integrity of the base material. At an exposure period of 500hr, the thickness of the oxide layer is approximately 1 µm, while the thickness of the Mo enriched layer containing the pores is approximately 2μm. Based on a total thickness of 3µm, the corrosion rate was calculated to be 0.05mm/year.

Careful observation of the EDS maps in Figures 5b through 5f show that Cr is depleted in this region. Consequently, our hypothesis is that the pores are a result of the diffusion of Cr toward the surface to form the outer oxide layer, causing contraction of the base material at the interface between the base alloy and the oxide layer. As corrosion proceeds, the diffusion of Cr from the bulk alloy becomes the limiting factor, and the surface of these voids then offer the path of least resistance to allow reaction of Cr with the salt to form the Cr-based oxide layer. The increased volume of the oxide eventually fills in the void space. The growth and subsequent infill of these voids may give rise to the multi-layered oxide structure observed on the samples exposed to identical conditions for 1000hr in Figure 6. The lack of voids observed in Figure 6 may be due to the path required for diffusion of Cr from the alloy. This is supported by near complete depletion of Cr in the Ni and Fe rich layers between the Cr-based oxides.

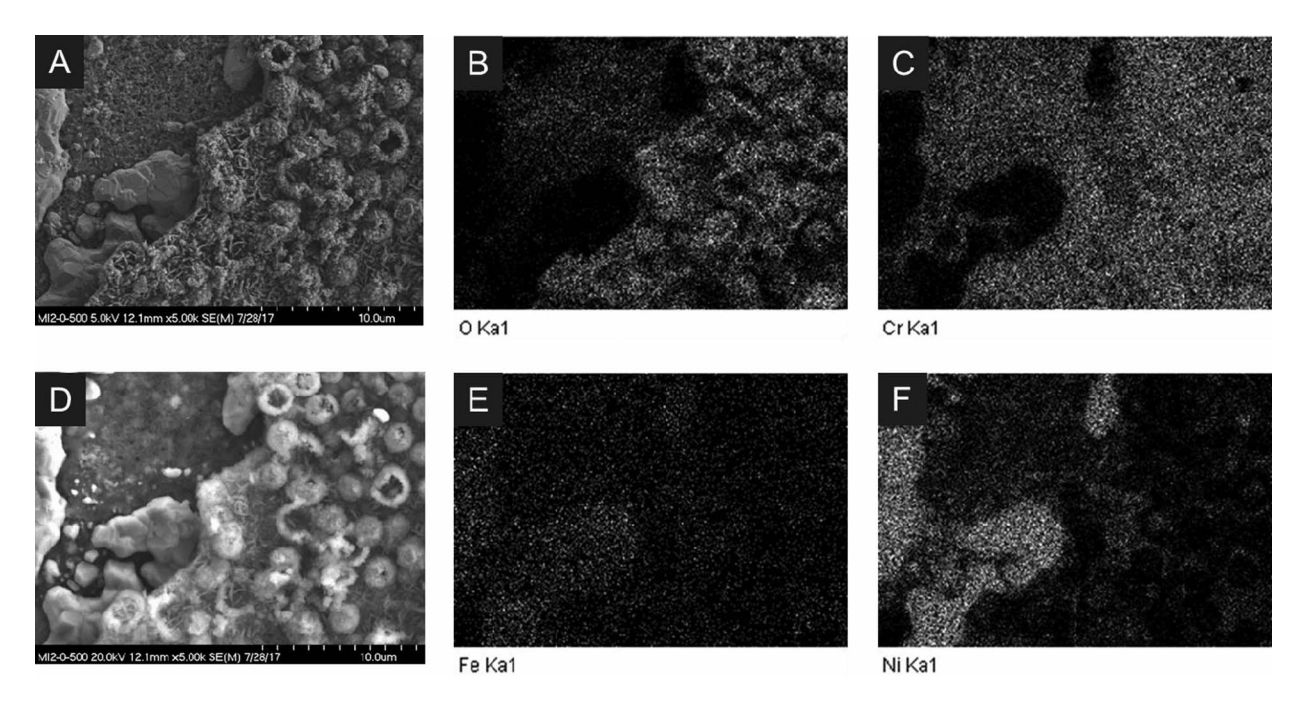


Figure 4. SEM images and EDS maps of the same area for the I625 sample exposed to LiCl- $2wt\%Li_2O-0wt\%Li$ for 500hr. (A) SEM micrograph same as in Figure 3B given for reference, taken at 5kV accelerating voltage, (B) EDS map of O K α , (C) EDS map of Cr K α , (D) SEM micrograph of same area, taken at 20kV accelerating voltage (E) EDS map of Fe K α , and (F) EDS map of Ni K α . For the EDS maps, lighter tones indicate higher concentrations of that element.

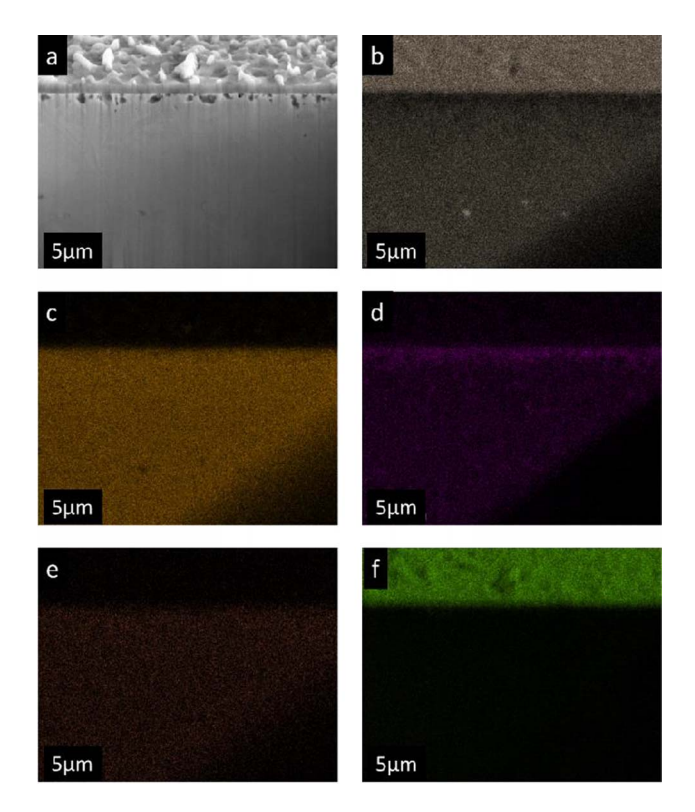


Figure 5. SEM micrograph (a) and EDS mapping analysis of the FIB milled trench on the I625 sample exposed to LiCl-1wt%Li₂O-0wt%Li for 500hr showing variations in concentration of (b) Cr, (c) Ni, (d) Mo, (e) Fe, and (f) O. The sample surface is observed as the image was taken at an angle of 52° from normal to the plane of the sample. The delineation between sample surface and cross section is demarked by the location of the abrupt change in intensity of all elements. Cr is seen to be enriched on the surface of the sample, while Mo is slightly enriched just below the outer corrosion layer. Oxide thickness is approximately $1\mu m$, while the depth to the bottom of the lowest void space is $2.25\mu m$.

For the I625 sample exposed to LiCl-1wt%Li₂O-0wt%Li for 1000hr, the corrosion rate was approximately 0.07mm per year, indicating that corrosion was approximately linear for these experiments. The oxide film was well developed, and showed a multi-layered structure similar to that shown for the I625 sample exposed to LiCl-2wt%Li₂O-0wt%Li for 500hr in Figures 3 and 4. The Mo enriched layer below the outer corrosion layer was still observed, however, there were no voids located in this area as there were on the 500hr sample. Mo accumulation was also observed at the grain boundaries, along with Cr and Nb, which is likely due to thermal aging of the microstructure, rather than a result of exposure to the molten LiCl-Li₂O solution. 39 Although enrichment of Cr, Mo, and Nb were observed along the grain boundaries, carbon was not observed at these locations, so it cannot be concluded that sensitization was observed. Corrosion did not proceed along the grain boundaries, so it seems that the enrichment of the grain boundaries in Cr, Mo, and Nb did not negatively impact the observed corrosion rate. However, sensitization followed by intergranular corrosion was observed in our previous work on SS316L under similar conditions.³⁶

As was observed via SEM imaging of the sample surfaces, the cross sections of the I625 samples exposed to LiCl-Li₂O in the presence of Li were consistent in morphology and showed an outer layer of a highly porous Ni rich foam-like structure. The formation of this porous layer is believed to be a result of the selective dissolution of Cr, Mo, and Nb from the base material, leaving the Ni-Fe matrix in place, similar to the formation of Rainey Nickel by the selective dissolution of Al from Ni-Al alloys. 40 This mechanism is likely similar to the void formation observed in Figure 5a, as diffusion of elements within the alloy is unlikely to be affected by the solution chemistry. The SEM images of the cross sections of the I625 samples exposed to LiCl-1wt%Li₂O containing 0.3, 0.6, or 1wt% Li at 650°C for 500 and 1000hr are shown in Figure 7. For the sample exposed to LiCl-1wt%Li₂O-0.3wt%Li for 500hr, the porosity penetrated into the surface to a depth of approximately 30µm, corresponding to a corrosion rate of 0.53mm/year. However, all other samples consistently showed a penetration depth of 15 µm, regardless of Li concentration or period of exposure, indicating that a direct measure of the corrosion rate is not necessarily applicable for these specimens. The similarity in the morphology and depth of attack regardless of Li concentration or

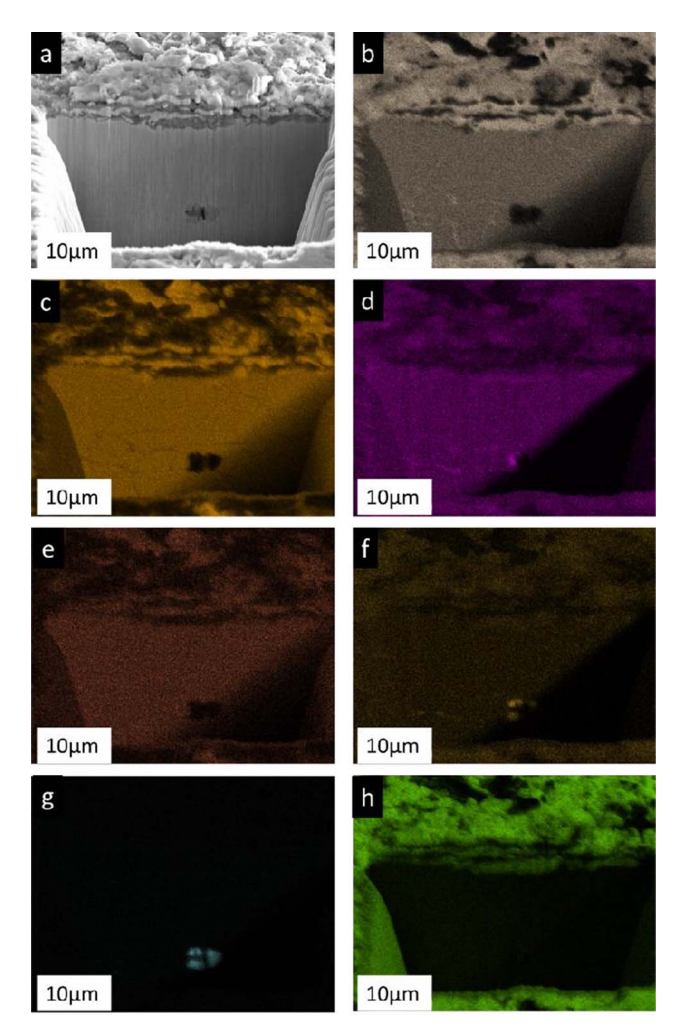


Figure 6. SEM micrograph (a) and EDS mapping analysis of the FIB milled trench on the I625 sample exposed to LiCl-1wt%Li₂O-0wt%Li for 1000hr showing variations in concentration of (b) Cr, (c) Ni, (d) Mo, (e) Fe, (f) Nb, (g) Ti, and (h) O. The multi-layered structure observed here corresponds to a similar oxide layer structure observed in Figures 3 and 4. Again, Mo enrichment is seen immediately below the corrosion layer, without significant incorporation of Mo into the oxide layer itself. The precipitate seen at a depth of $17\mu m$ consists largely of Ti, Mo, and Nb. Cr, Mo, and Nb were also observed to be enriched along the grain boundaries.

exposure period indicates that there may be a threshold concentration of Li necessary to cause this morphology and that threshold is likely below 0.3wt%, and the reactions responsible for pore formation may not be diffusion controlled. Further studies at Li concentrations below 0.3wt% would be necessary to determine at what concentration this morphology begins to be observed as well as the mechanisms responsible for pore formation. Due to the presence of metallic Li, liquid metal embrittlement may play a role in the formation of the microstructures observed here, although verification of this hypothesis would require further investigation.

The variation in composition as a function of depth was investigated via EDS of the cross sections. As all samples exposed to LiCl-Li $_2$ O in the presence of Li displayed similar variations in composition, the SEM-EDS results for the I625 sample exposed to LiCl-1wt%Li $_2$ O-1wt%Li at 650°C for 1000hr are shown in Figure 8, while spot EDS analysis for the locations shown in Figure 8a are given in Table II. Cr, Mo, and Nb are all significantly depleted from the material remaining in the porous layer, leaving primarily Ni, with Fe remaining at approximately the same ratio as in the base material. The depletion of Cr, Mo, and Nb was also observed to irregularly penetrate into the sample beyond the depth of the porous layer. The loss of the amount

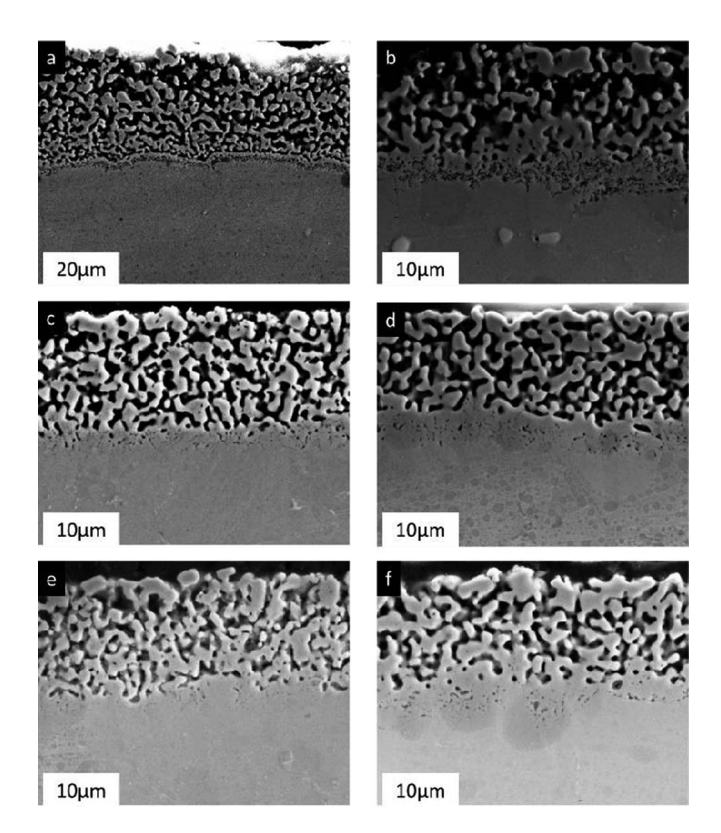


Figure 7. Cross section SEM images for I625 samples exposed to LiCl-1wt%Li₂O containing 0.3wt% Li for (a) 500hr or (b) 1000hr, 0.6wt%Li for (c) 500hr or (d) 1000hr, or 1wt%Li for (e) 500hr or (f) 1000hr. The porous microsctructure observed via SEM of the sample surface was also observed in cross section, and was consistent amongst sample exposed to LiCl-Li₂O in the presence of Li.

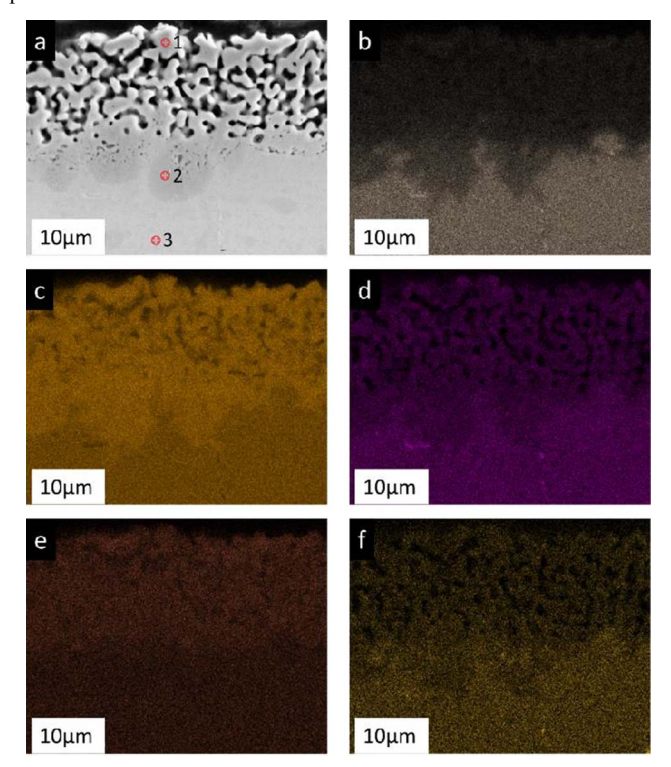


Figure 8. SEM micrograph (a) and EDS mapping analysis of the cross section of the I625 sample exposed to LiCl-1wt%Li₂O-1wt%Li for 1000hr showing variations in concentration of (b) Cr, (c) Ni, (d) Mo, (e) Fe, and (f) Nb. Locations marked 1, 2, and 3, were analyzed via point analysis, which is presented in Table II.

Table II. EDS spot analysis of the locations demarked in Figure 8a for the I625 sample exposed to LiCl-1wt%Li₂O-1wt%Li for 1000hr. The outermost layer was depleted in Cr compared to the base material, while the dark spots seen in some locations on these samples did not show any observable variation in composition compared to the base material.

Element	Spot 1 (wt%)	Spot 2 (wt%)	Spot 3 (wt%)
Nb	-	2.87	2.97
Mo	4.86	7.18	7.19
Cr	5.31	22.34	23.7
Fe	8.35	5.17	5.17
Ni	81.48	62.45	60.98

of Cr, Mo, and Nb necessary to reach the composition of spot 1 shown in Figure 8a represents the loss of a significant fraction of the material, which may account for the porous microstructure seen on this sample and other I625 samples exposed to LiCl-Li₂O in the presence of Li.

Conclusions

I625 samples were exposed to molten LiCl solutions containing 1 or 2wt% Li₂O and 0, 0.3, 0.6, or 1wt% Li maintained at 650°C for periods of 500 and 1000hr to investigate the effect of metallic Li on the degradation of the material. In the absence of metallic Li, I625 formed a highly crystalline, stable oxide film with a multi-layered structure that limited corrosion to approximately 0.05 to 0.07mm/year. The presence of metallic Li in solution prevented the formation of any substantial oxide film, resulting in a highly porous, foam-like structure. The depletion of Cr, Mo, and Nb from the surface was also observed on these samples via EDS, indicating that these elements were preferentially leached from the base material by the molten solution. The loss of these elements from the sample surface, which together constitute one-third of the material, is likely responsible for the highly porous microstructure observed.

Acknowledgments

This work was performed under the auspices of the Department of Energy (DOE) under contracts DE-NE0008262 and DE-NE0008236, and the US Nuclear Regulatory Commission (USNRC) under contracts NRCHQ-11-G-38-0039 and NRC-HQ-13-G-38-0027. W.P. acknowledges the Fellowship Award from the USNRC. Dr. Kenny Osborne serves as the program manager for the DOE award and Nancy Hebron-Isreal serves as the grants program officer for the NRC awards.

ORCID

Dev Chidambaram https://orcid.org/0000-0002-3918-3559

References

J. J. Laidler, J. E. Battles, W. E. Miller, J. P. Ackerman, and E. L. Carls, *Progress in Nuclear Energy*, 31, 131 (1997).

- K. Gourishankar, L. Redey, and M. Williamson, Electrolytic Reduction of Metal Oxides in Molten Salts, in: W. A. Schneider (Ed.) Light Metals, The Minerals, Metals & Materials Society, 2002.
- S. D. Herrmann, S. X. Li, and M. F. Simpson, Electrolytic Reduction of Spent Oxide Fuel - Bench-Scale Test Results, GLOBAL 2005, Tsukuba, Japan, 2005.
- H. Lee, G.-I. Park, K.-H. Kang, J.-M. Hur, J.-G. Kim, D.-H. Ahn, Y.-Z. Cho, and E. H. Kim, *Nuclear Engineering and Technology*, 43, 317 (2011).
- S. D. Herrmann, S. X. Li, M. F. Simpson, and S. Phongikaroon, Separation Science and Technology, 41, 1965 (2006).
- M. Kurata, T. Inoue, J. Serp, M. Ougier, and J. P. Glatz, *Journal of Nuclear Materials*, 328, 97 (2004)
- S. M. Jeong, H. S. Shin, S. H. Cho, J. M. Hur, and H. S. Lee, *Electrochimica Acta*, 54, 6335 (2009).
- S. X. Li, M. F. Simpson, and S. D. Hermann, Oxygen Ion Oxidation Process on a Platinum Electrode in LiCl-Li₂O At 650C, in: R. A Mantz (Ed.) Electrochemical Society Proceedings, vol 24, 2004.
- A. Merwin, M. A. Williamson, J. L. Willit, and D. Chidambaram, *Journal of the Electrochemical Society*, 164, H5236 (2017).
- W. Park, J.-M. Hur, S.-S. Hong, E.-Y. Choi, H. S. Im, S.-C. Oh, and J.-W. Lee, *Journal of Nuclear Materials*, 441, 232 (2013).
- A. Merwin, W. C. Phillips, M. A. Williamson, J. L. Willit, P. N. Motsegood, and D. Chidambaram, *Scientific Reports*, 6, 25435 (2016).
- A. S. Dworkin, H. R. Bronstein, and M. A. Bredig, The Journal of Physical Chemistry, 66, 572 (1962).
- 13. M. A. Bredig, Mixtures of Metals with Molten Salts, United States, 1963.
- L. M. Ferris, M. A. Bredig, and F. J. Smith, *The Journal of Physical Chemistry*, 77, 2351 (1973).
- 15. T. N. Nakajima and N. Watanabe K., Nippon Kagaku Kaishi, 1974, 401 (1974).
- T. Nakajima, R. Minami, K. Nakanishi, and N. Watanabe, Bulletin of the Chemical Society of Japan, 47, 2071 (1974).
- T. N. Nakajima and N. Watanabe K., Bulletin of the Chemical Society of Japan, 49, 994 (1975).
- T. Nakajima, K. Nakanishi, and N. Watanabe, Nippon Kagaku Kaishi, 1975, 617 (1975).
- A. J. Burak and M. F. Simpson, JOM, 68, 2639 (2016).
- S. H. Cho, J. S. Zhang, Y. J. Shin, S. W. Park, and H. S. Park, *Journal of Nuclear Materials*, 325, 13 (2004).
- R. Y. Liu, X. Wang, J. S. Zhang, and X. M. Wang, Journal of Nuclear Materials, 327, 194 (2004).
- C. Soo-Haeng, L. Jong-Ho, P. Sung-Bin, J. Ki-Jung, and P. Seong-Won, *Journal of the Korean Institute of Metals and Materials*, 43, 449 (2005).
- 23. Q. Gao, R. Y. Liu, J. S. Zhang, and J. T. Guo, Materials Letters, 59, 2052 (2005).
- C. Soo-Haeng, P. Seong-Bin, L. Jong-Hyeon, H. Jin-Mok, and L. Han-Soo, Oxidation of Metals, 78, 153 (2012).
- P. SangKyu, L. TaeHyuk, S. MoonSoo, N. JaeSoo, C. SooHaeng, and L. JongHyeon, Advanced Materials Research, 886, 41 (2014).
- S.-H. Cho, S.-K. Lee, D.-Y. Kim, J.-H. Lee, and J.-M. Hur, *Journal of Alloys and Compounds*, 695, 2878 (2017).
- T. R. Allen and K. Sridharan, Corrosion in Molten Salts, in Molten salts chemistry from lab to applications, Elsevier, Burlington, MA, 2013.
- 28. Y. S. Zhang, Journal of The Electrochemical Society, 133, 655 (1986).
- J. E. Indacochea, J. L. Smith, K. R. Litko, and E. J. Karell, *Journal of Materials Research*, 14, 1990 (1999) M1993 1910.1557/JMR.1999.0268.
- B. Mishra and D. L. Olson, Mineral Processing and Extractive Metallurgy Reviews, 22, 369 (2001).
- 31. A. Merwin and D. Chidambaram, Corrosion Science, 126, 1 (2016).
- 32. A. Merwin and D. Chidambaram, Nuclear Technology, 195, 204 (2016).
- W. Phillips, A. Merwin, and D. Chidambaram, Metallurgical and Materials Transactions A, 49, 2384 (2018).
- 34. E.-Y. Choi and J. Lee, Journal of Nuclear Materials, 495, 85 (2017).
- A. Merwin, Material Interactions with Molten LiCl-Li₂O-Li, Materials Science and Engineering, vol Doctor of Philosophy in Materials Science and Engineering, University of Nevada, Reno, 2016, p. 241.
- 36. W. Phillips and D. Chidambaram, Journal of Nuclear Materials, 517, 241 (2019).
- N. J. Gese, The Electrochemistry of Li-LiCl-Li₂O Molten Salt Systems and the role of Moisture, Nuclear Engineering, University of Idaho, 2015.
- W. Phillips and D. Chidambaram, Journal of the Electrochemical Society, (Under Review).
- S. Malej, J. Medved, B. Šetina Batič, F. Tehovnik, and M. Godec, Microstructural evolution of inconel 625 during thermal aging, 2017, p. 319.
- H. Lei, Z. Song, D. Tan, X. Bao, X. Mu, B. Zong, and E. Min, Applied Catalysis A: General, 214, 69 (2001).